Macromolecules

Article

Cite This: Macromolecules 2018, 51, 3597−3607

Temperature-Dependent Nanoparticle Dynamics in Poly(*N*-isopropylacrylamide) Gels

Emmabeth Parrish, Sarah C. Seeger, and Russell J. Composto*

Department of Materials Science and Engineering, School of Engineering and Applied Science, University of Pennsylvania, Philadelphia, Pennsylvania 19104, United States

ABSTRACT: Nanoparticle (NP) probes were used to characterize the local structure of *N*-isopropylacrylamide (NIPAAM), a thermoresponsive hydrogel, using single particle tracking (SPT). Swelling ratio, and thus gel network confinement, was varied by tuning polymer and cross-linker concentrations. Based on the swelling ratio, the volume phase transition (VPTT) was determined to be near 32 °C. In general, NPs were found to be localized by two barriers. A primary localization region of approximately 100 nm was attributed to attractive interactions between the NIPAAM strands and the poly(ethylene glycol) (PEG) brush grafted to the NP. As the polymer and cross-linker concentrations were reduced, or temperature approached the VPT, NPs escape the primary localization region and explore a larger secondary localization region (150−300 nm), ascribed to confinement by the gel network. As temperature was raised above the VPT, however, the increase in confinement due to the collapse of the NIPAAM strands dominated, causing NPs to become localized to a single region despite the higher temperature. This study of NP dynamics provides insight into controlling the release and loading of drugs in responsive hydrogel systems.

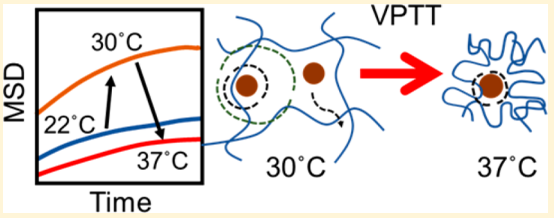

INTRODUCTION

Stimuli-responsive gels are polymer networks in which properties change based on environmental cues such as pH, temperature, or electric field. Because their high water content and low interfacial tension enable biocompatibility, responsive hydrogels have drawn interest from biomedical fields. Further, these hydrogels have potential for biotechnological applications such as biosensors, bioseparation, and immobilization of enzymes in the body. Because these materials can actuate in response to stimuli, they could also be used to pump drugs into or from desired areas or selectively allow for drug permeation.[1] Controlling the diffusion and localization of drugs in such applications is critical to the functionality. *N*-Isopropylacrylamide (NIPAAM), a well-studied temperature-responsive hydrogel, exhibits a lower critical solution temperature (LCST) and undergoes a phase transition near 32 °C, slightly below body temperature, making it a desirable candidate for these biomedical applications.[1−3] In this study, we probe the mobility of nanoparticles (NPs) within NIPAAM at temperatures below and above the LCST. Understanding and controlling the diffusion of nanoscale particles within gels is important to aid in the implementation of these biomedical applications.

Below the LCST, called the volume phase transition temperature (VPTT) in hydrogels, NIPAAM gels are water-swollen because of the hydrophilic interaction between water and amide groups in the polymer chain.[2] As the temperature is raised, the entropic costs of interactions with hydrophobic hydrocarbon and isopropyl groups of the polymer cause the NIPAAM chain to begin to expel water.[2−4] At the VPTT, the association between hydrophobic groups dominates, resulting in chain collapse and a sharp decrease in gel volume. As a result, pore, or mesh, size displays a large temperature dependence in NIPAAM gels.[5,6] Small-angle neutron scattering (SANS) studies on NIPAAM gels suggest that the mesh size at room temperature is on the order of a few nanometers.[5,7,8] The correlation length scales with polymer concentration to the −1.16 power for NIPAAM gels; however, for concentrations from 0.009 to 0.2 polymer fraction this only changes the mesh from approximately 1 to 5 nm.[8] Using a gel filtration method to estimate the pore size of NIPAAM gels cross-linked with bis(acrylamide) (bis) and acrylamide, a study by Park and Hoffman[9] claimed that NIPAAM pore size decreased to below the molecular size of vitamin B12 (MW 1355 Da, ∼3 nm[10]) at temperatures above the VPTT, ∼35 °C. Although mesh size represents the average space between polymer chains in the water-filled gel, the pore structure is heterogeneous, and this heterogeneity can have a large impact on gel properties, such as modulus.[11]

To better control the capture and release of drugs and other small molecules within hydrogels being used in applications such as drug delivery systems, the local environment within the gel must be well understood. A gel's formation causes several types of inhomogeneities to be present within the gel, as stated by Shibayama and Norisuye: spatial inhomogeneities induced by variations in cross-linking across different areas of the gel, mobility inhomogeneities due to local variations in mobility of the cross-linked chains, connectivity inhomogeneities dependent on the distribution of polymer chains throughout the gel, and topological inhomogeneities due to defects in the gel network.[12] Gels prepared with low polymer and cross-linker

Received: February 12, 2018
Revised: April 24, 2018
Published: May 2, 2018

DOI: 10.1021/acs.macromol.8b00335
Macromolecules 2018, 51, 3597−3607

concentrations have inconsistent properties, such as modulus and swelling ratio, as the effective polymer and cross-linker concentrations differ throughout the gel. As cross-linking density is increased, however, the amount of spatial and mobility inhomogeneities increases. Analogously, higher polymer concentration can allow for more variation in polymer distribution, leading to higher connectivity inhomogeneity.[13] Chetty et al.[11] found that in a NIPA/bis system, increasing cross-linker content from 1.1 to 3.3 mol % bis led to higher elastic moduli, from 4 to 8 kPa, but at 9.1 mol % bis, structure inhomogeneity caused the modulus to be anomalously low, 2 kPa. Sayil and Okay found that a cross-linker content of 3 mol % was the upper limit for structure homogeneity in NIPA/bis systems, above which they observed agglomeration of NIPAAM gel microspheres and a corresponding decrease in modulus, from 12 to 2 kPa at 3 and 5 mol % bis, respectively, an indication of system heterogeneity.[14]

Polymer concentration and cross-linking density also affect the volume phase transition. Increasing either polymer or cross-linker concentration yields a more tightly knit gel structure in which there is a reduced capacity for retention of water and thus for swelling.[15] When cross-linking is increased, the VPTT remains unchanged despite these differences in swelling ratio because the rate-limiting step for swelling and deswelling is mass transfer of the water entering and exiting the gel.[1,15,16] A highly cross-linked gel has a lower swelling ratio, so less water must leave the gel as the temperature is raised above the VPTT, offsetting the decreased rate of mass transfer due to confinement of the system. As polymer concentration is increased, however, the VPTT becomes sharper.[17] At higher polymer concentrations, hydrophobic interactions are stronger, driving the VPTT to be lower and to occur over a narrower range in temperature.[17]

Although the VPTT of NIPAAM has been extensively studied, an effective model for predicting the mobility of molecules within these gels remains elusive. Peppas and Reinhart introduced the first model for diffusion in chemically cross-linked hydrogels, in which they propose that diffusion is proportional to the mesh size of a gel, which is dependent on swelling.[18,19] While this model has been shown to predict diffusion effectively for solutes much smaller than the mesh size, theoretical predictions become inaccurate as the diffusant size nears, or becomes larger than, the mesh size of the gel.[20] Other models, such as the hydrodynamic[21] and obstruction[22] models, have since been developed in attempts to improve upon the free volume model. However, each of these models has their own limitations: the hydrodynamic model, which treats the diffusing solute as a large molecule for which diffusion is resisted by a large drag force, does not take into consideration heterogeneity in the gel; obstruction theory, which takes into account that the gel network contains polymer chains that the diffusant cannot bypass, works well for heterogeneous systems but assumes rigid, motionless polymer chains, far from the dynamic network of mobile polymer chains that exists in gels.[23] Additional models for NP diffusion in gels have sprung out of the polymer physics community; however, these models were largely developed to describe dry polymer networks.[24,25] In the absence of effective models to predict the diffusion of molecules in NIPAAM hydrogels, some attempts have been made to directly determine the uptake and release of drugs into NIPAAM hydrogels in vitro.[17,26] In these studies, however, the local environment that the drug experiences was not characterized, and the drugs were too small to act as probes.

In this work, single particle tracking (SPT) was used to determine the mobility of quantum dot nanoparticles (NPs) functionalized with poly(ethylene glycol) (PEG) brushes (hydrodynamic diameter ∼10 nm) in a NIPAAM hydrogel system. The NPs act as probes to the system, allowing characterization of the local structural environment of the NIPAAM gel as the swelling ratio was tuned by varying either polymer or cross-linker concentrations or temperature. NPs were found to be localized by two barriers, resulting in a primary localization region of ∼100 nm caused by attractive interactions between the NP brush and the NIPAAM chains and a secondary localization region, from 150 to 300 nm, attributed to network confinement. As polymer and cross-linker concentrations were reduced, NP mobility increased, mainly due to an increase in the size of the secondary localization region. Additionally, as the temperature was increased toward the VPTT, the secondary localization region increased, resulting in an increase in escape of NPs from the region, even as the gel was beginning to collapse. As the temperature was raised above the VPTT, however, the increasing confinement caused by the collapse of the gel dominated, resulting in decreased motion and a single localization region, despite the increase in thermal energy. Understanding the impact of swelling and temperature on NP mobility within hydrogels will aid in the development of responsive gels for controlled release devices as precisely controlling nanoscale diffusants is paramount to functionality.

EXPERIMENTAL SECTION

Materials. *N*-Isopropylacrylamide monomer, *N*,*N*′-methylenebis(acrylamide), *N*,*N*,*N*′,*N*′-tetramethylethylenediamine (TEMED), glutaraldehyde, ammonium persulfate, dichlorodimethylsilane (DCDMS), and 3-aminopropyltriethoxysilane (APTES) were purchased from Sigma and were used as received.

Gel Preparation. Coverslips and glass slides were piranha (7v/3v sulfuric acid to hydrogen peroxide) cleaned. Glass slides were made hydrophobic, preventing adhesion of NIPAAM hydrogels, through overnight exposure to 1 mL of DCDMS. Coverslips were surface functionalized for 6 h minimum at 70 °C via 1 mL of APTES. Coverslips were then incubated in 0.5% v/v glutaraldehyde to water. NIPAAM gels were produced by free radical polymerization using bis as a hydrophilic cross-linker.[17] Solutions of NIPAAM/bis were prepared in water with varying concentrations well above the gelation threshold of 100−150 mM NIPAAM for bis content of 2−5 mM.[27] The three conditions used were 30/0.5 (low swelling), 20/0.5 (intermediate swelling), and 20/0.4 (high swelling) which corresponds to mg/mL NIPAAM/bis. Solutions were chilled for at least 30 min to slow reaction and increase homogeneity of gels. The solutions were then deoxygenated with nitrogen for a minimum of 30 s, and 10 μL of ammonium persulfate (10% w/v) and 2.5 μL of TEMED were added per milliliter of solution to initiate cross-linking. 30 μL of the mixed gel solution was subsequently pipetted onto separate glass slides. Quantum dot CdSe/ZnS/CdS NPs (core 4 nm, hydrodynamic diameter 10 nm) were synthesized according to previously established procedures (precursors: 1 mL of 0.5 M CdS, 1 mL of 0.5 M S solutions)[28] and were surface functionalized with 5K PEG and dispersed in water at 0.001−0.025 nM. 0.5 μL was added to the gel solution. A coverslip was placed on top, causing the gel solution to spread and form thin 20−40 μm gels over the complete area of the coverslip. Samples were then exposed to a 100 W Spectroline SB-100PX high-intensity ultraviolet lamp (wavelength of 365 nm) at 1 foot for a minimum of 8 h. Following gelation, samples were swollen in DI water for 36 h. Bulk gel samples were prepared as discs of 25 mm diameter and swollen in water for 48 h before testing.

DOI: 10.1021/acs.macromol.8b00335
Macromolecules 2018, 51, 3597−3607

Table 1. Sample Characteristics Including Polymer Concentrations, Molar Mass between Cross-Links (M_c), Distance between Cross-Links in Unswollen Gel (r), Swelling Ratio (Q), and Swollen Mesh Size, ξ (Values Obtained from $n \geq 2$ Samples)

gel code	temp (°C)	mg/mL		M_c (g/mol)	r (nm)	Q	swollen ξ (nm)
low	22	NIPA	30	9406	5.2	50	19
		bis	0.5				
intermediate	22	NIPA	20	6322	4.3	110	20
		bis	0.5				
	25					110	20
	30					85	19
	37					2	5
high	22	NIPA	20	7864	4.8	280	31
		bis	0.4				

Swelling Measurements. Bulk gel samples were swollen in a DI water bath at the appropriate temperature (22−40 °C) using a Fisher Scientific Isotemp system for a minimum of 12 h. Gels were transferred to a dry glass container and weighed to determine swollen weight at each temperature. The swelling ratio was calculated as follows:

$$Q = \frac{w_t}{w_d} \tag{1}$$

where w_d represents the dried weight of the gel (approximated as the weight of the gel at the highest temperature, 40 °C), and thus minimal swelling, and w_t represents the swollen weight of the gel at each temperature. For each condition, at least two independent experiments were performed on different days.

Single Particle Tracking and Analysis. A Nikon Eclipse Ti inverted optical microscope with a 100× 1.49 NA objective on an optical table was used to perform the SPT experiments. The QDs were excited with a 532 nm laser beam. The frame rate was set to 40 ms. Samples were placed in the AFM Bioheater closed fluid cell and filled with NP solution. Samples were then heated to the appropriate temperature, beginning at 22 °C (precision: 0.02 °C; accuracy: 0.1 °C). Coverslip and gel surface positions were noted, and videos were taken at positions at least 5 μm from either side of the gel surface. A CCD camera (Cascade-512B, Photometrics) was used to collect 40 s videos at a rate of ∼25 frames/s.

FIESTA (Fluorescence Image Evaluation Software for Tracking and Analysis), a MATLAB-based particle tracking software package, was used to extract particle trajectories from videos through two-dimensional Gaussian fits of fluorescence intensity.[29] Conditions for particle tracking were as follows: FWHM of the fluorescence intensity profile was initialized at 900 nm, ∼8 pixels, 8 frame minimum, 4 frame break allowable. Postprocessing removed trajectories where the average error was greater than 25 nm or containing jumps larger than 2000 nm (i.e., linking nearby particles). Experimental drift was less than positioning error as determined by imaging immobilized NPs.

The publicly available MATLAB program msdanalyzer[30] was used along with personally developed MATLAB codes to determine NP's spatial coverage, MSD, van Hove distributions, and localization regions. MSD, the expected value for the distance traveled by a particle in a given amount of time, was calculated according to the equation

$$\mathrm{MSD} = \langle r(\tau)^2 \rangle = \langle (r(t+\tau) - r(t))^2 \rangle \tag{2}$$

It is notable that the number of tracks decreases as time increases, since all tracks are initialized at 0 s. Tracks that exist at longer times tend to be representative of particles that are more localized; since tracks for particles that are more mobile are rarer at longer times, MSDs at those times are often skewed toward the localized, or immobile, particles. To prevent bias, we limit our analysis to relatively short time scales (∼1 s).

RESULTS AND DISCUSSION

This study used SPT to probe the mobility of PEG functionalized NPs within NIPAAM networks as confinement was tuned by varying either the polymer and cross-linker concentrations or temperature. At 22 °C, three combinations of polymer to cross-linker ratios were studied: 30/0.5, 20/0.5, and 20/0.4 mg/mL of NIPAAM/bis, which are denoted as low, intermediate, and high swelling gels. SPT was also performed on the intermediate swelling gel for temperatures from 22 to 37 °C. The expected mesh sizes are calculated from the observed swelling ratios. The results of the SPT experiments were analyzed by their spatial coverage, mean-squared displacements (MSD), and displacement distributions.

Mesh Size and VPTT of NIPAAM Gels. To probe the effect of polymer concentration, cross-linker concentration, and temperature on both the VPTT and mobility of NPs within NIPAAM gels, three different gels were prepared at two cross-linker and two polymer concentrations. The gel characteristics are summarized in Table 1. Gels are designated by their swelling ratio, Q, as low, intermediate, and high, which correspond to 30/0.5, 20/0.5, and 20/0.4 mg/mL of NIPA/bis, respectively, in the gelling solution. Increasing either the polymer or cross-linker concentration resulted in a decrease in mesh. The distance between two cross-links, r, can be calculated based on the initial concentrations of monomer and cross-linker using eq 3[31]

$$r = l\left(\frac{2M_c}{M}\right)^{1/2} C_n^{1/2} \tag{3}$$

where l is the length of a carbon−carbon bond, M_c is the molar mass between cross-links, M is the molar mass of a monomer, and C_n is the characteristic ratio of the polymer (6.9).[31] M_c can be calculated from eq 4[31]

$$M_c = \frac{n(\mathrm{NIPA})}{n(\mathrm{bis})} M(\mathrm{NIPA}) + M(\mathrm{bis}) \tag{4}$$

where n designates the number of moles used and M designates the molar mass of NIPA or bis. The mesh size in the swollen gel can then be calculated from eq 5[31]

$$\xi = \frac{r}{v^{1/3}} \tag{5}$$

where v is the polymer volume fraction, or inverse of the swelling ratio, Q. Equation 5 assumes the gels are highly swollen so that the density of the gel is approximated as that of water. For the range of polymer and cross-linker concentrations used in this study, the value of r changed very little, from 4.3 to 5.2 nm. The expected mesh size in the swollen state, however, changed by over 10 nm due to the disparate swelling of the gels.

The swelling ratio of the high, intermediate, and low swelling gels over the temperature range 22−40 °C is shown in Figure 1.

DOI: 10.1021/acs.macromol.8b00335
Macromolecules 2018, 51, 3597−3607

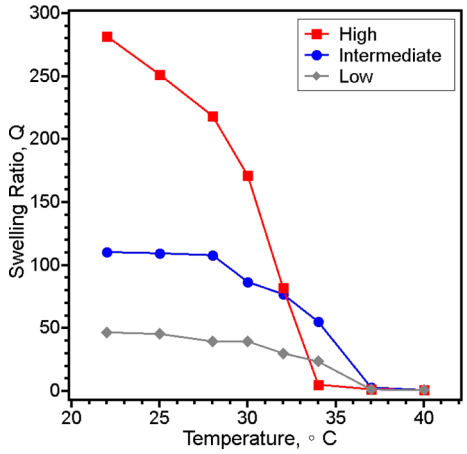

Figure 1. Swelling ratio for NIPAAM gels of high (red), intermediate (blue), and low (gray) swelling over the temperature range 22−40 °C.

The high swelling gel, shown in red, had a swelling ratio of 280 at 22 °C. The swelling ratio remained above 200 until 30 °C and then drastically decreased, stabilizing at 34 °C. The intermediate swelling gel, shown in blue, had a swelling ratio of 110 until 28 °C. The swelling ratio decreased from 110 to 60 between 28 and 34 °C. The gel then reached the collapsed state at 37 °C. The low swelling gel, shown in gray, had a swelling ratio of 50 until 30 °C, which decreased from 30 to 35 °C and reached the collapsed state at 37 °C. As expected, the high swelling gel shows the sharpest transition near the VPTT, as previously observed.[17] At 22 °C, the swelling ratio decreased by over 200 from the low to high swelling gels with a change of less than 1 mol % of cross-linker and polymer. The decreased swelling ratio reduced the calculated mesh size from 31 to 18 nm, as seen in Table 1. Importantly, the swelling ratio controlled the mesh; despite the higher r value of the low swelling gel, the mesh was smaller than in the other two samples.

As discussed in the Introduction, the gel swelling ratio decreased upon increasing either polymer or cross-linker concentrations. While the swelling ratios of the gels differ greatly, the temperature range of the VPTT was similar for all three gels, occurring between 30 and 34 °C. These values are consistent with literature values. Namely, 32 °C has been cited as the VPTT for NIPAAM gels in simulations,[2,3] whereas 30−35 °C has been reported experimentally.[5]

The average mesh sizes for the intermediate gel as a function of temperature are given in Table 1. This gel was used for probing the effect of temperature on NP mobility. The gel remained fully swollen until approximately 28 °C (Figure 1) with a calculated mesh size of 20 nm. As the swelling ratio decreased, the calculated mesh decreased only slightly, to 19 nm. The network collapsed above 34 °C, resulting in a reduction of mesh size to 5 nm at 37 °C. The NPs used in this study had a hydrodynamic diameter of 10 nm. Thus, the mesh size changed from larger than to smaller than the NP size as temperature increased from 22 to 37 °C.

The VPTT is controlled by competing thermodynamic contributions of mixing enthalpy and entropy. During the phase transition, the NIPAAM chains transition from a coiled, the hydrophilic state, to a globular, the hydrophobic state, shape due to the competition between hydrogen bonds and hydrophobic interactions.[2,3] In the swollen state, hydrogen bonds are formed between the amine and carbonyl groups of NIPAAM and water as well as intrapolymer hydrogen bonds between the same groups. As the temperature is raised, hydrogen bonds between water and NIPAAM are broken, while interchain hydrogen bonds are formed.[2,3] Hydrogen bonding with water increases the enthalpy of mixing but decreases the entropy of mixing. The transition occurs when entropy dominates at higher temperatures, making separation of water and network strands favorable.[32]

In Table 1, the mesh sizes were calculated based on idealized statistical copolymerization and thus do not capture the intrinsic heterogeneity of the NIPAAM gel structure. These mesh values provide a starting point for the discussion of the confinement experienced by the NPs within the various gel conditions. In the literature, the mesh size of NIPAAM depends on polymer and cross-linker concentrations as well as the

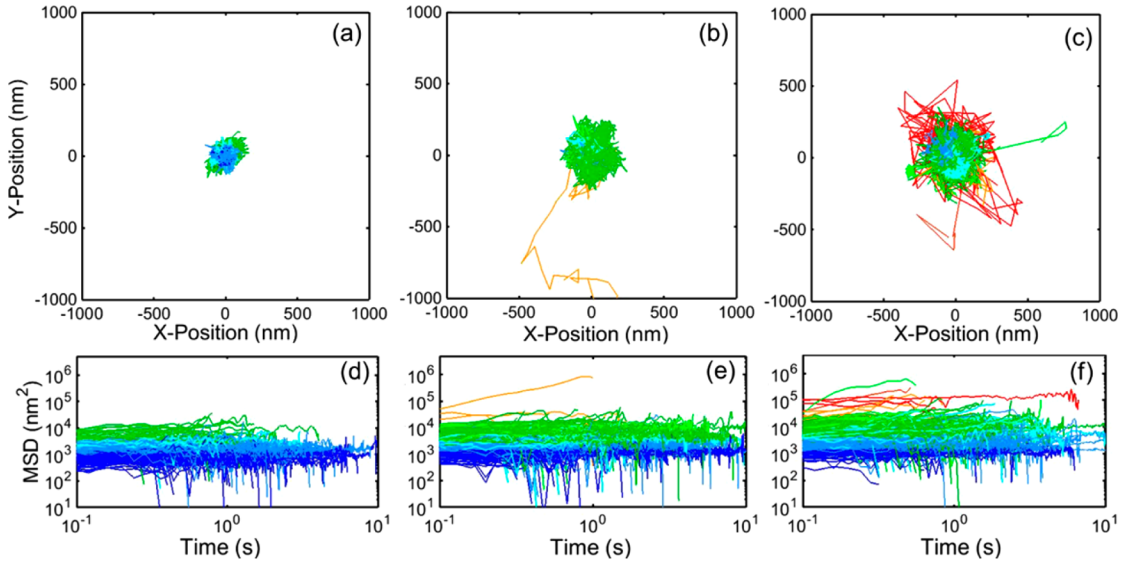

Figure 2. Trajectories of NPs in (a) low, (b) intermediate, and (c) high swelling gels at 22 °C (below VPTT), which have been initially centered at (0, 0). MSDs for individual tracks as a function of time in (d) low, (e) intermediate, and (f) high swelling gels. Line colors vary from blue to red with increasing initial MSD (showing $N \approx 500$).

DOI: 10.1021/acs.macromol.8b00335
Macromolecules 2018, 51, 3597−3607

method used to determine the mesh size. Thus, mesh sizes from different methods are only indirectly related to one another. Using SANS of NIPAAM gels, the average correlation lengths were found to be 2−3 nm.[5,7] Using dynamic light scattering (DLS), average correlation lengths ranging from 6 to 120 nm have been reported.[6] Both DLS and SANS measure averaged correlations lengths, with DLS measuring the intensity weighted dynamic correlation length and SANS measuring the static correlation length. The mesh sizes listed in Table 1 can be related to literature values of averaged correlation lengths of gels made with similar polymer content under similar conditions. The concentrations and conditions for gelation in this study are similar to those used in the DLS study,[6] and thus the calculated values are consistent with these literature values.

NP Mobility within NIPAAM Gels. *Effect of Increasing Cross-Linking on NP Mobility (T = 22 °C).* Figure 2a−c shows NP trajectories spatial coverage in x−y space for the high, intermediate, and low swelling gel conditions at 22 °C. The NPs in the low swelling gel were localized within a 100 nm radius, as shown in Figure 2a. The majority of NPs in the intermediate swelling gel were localized within a 200 nm radius, as shown in Figure 2b. In the high swelling gel the majority of NPs were localized within a 250 nm radius, as shown in Figure 2c. In all cases, the majority of NPs move within a localized region. To quantify the motion of these particles, the mean-squared displacement (MSD) of each particle is displayed in Figure 2d−f. To aid visualization, line colors vary from blue to red as the initial MSD values increased in Figure 2a−f. The average MSD value for the low swelling gel at 0.4 s was $10^{3.1}$ (35^2) nm^2. At the same time, the average MSD value for the intermediate and high swelling gels were $10^{3.4}$ (50^2) and $10^{3.7}$ (71^2) nm, respectively. The increased swelling and resulting free volume of the gels with lower polymer and cross-linking concentrations allowed NPs to move further within these gels.

Ensemble MSD curves (Figure 3), calculated by averaging the MSD curves from Figure 2, show increasing mobility of the

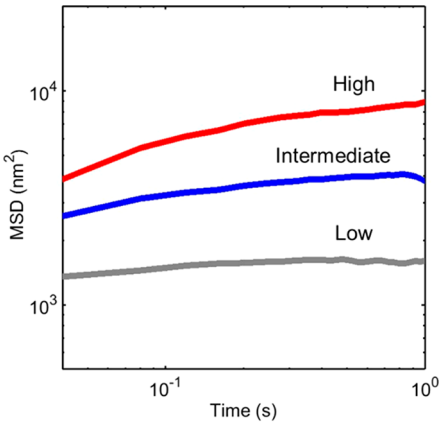

Figure 3. Ensemble NP MSD in high (red), intermediate (blue), and low (gray) swelling gels at 22 °C. Decreasing polymer or cross-linker content results in increased MSD of NPs.

NPs with increasing swelling ratio of the gel. The high, intermediate, and low swelling gels are shown in red, blue, and gray, respectively. At 0.4 s, the mean MSD value increased from 1600 (40^2) to 8000 (89^2) nm^2 from the high to low swelling gels. The MSD of Brownian diffusion is proportional to time; mathematically, this relationship can be described as t^{α}, where $\alpha = 1$. Figure 3 shows that for all polymer and cross-linker concentrations used in this study (20−30/0.4−0.5 mg/mL NIPAAM/bis), NPs moved in a subdiffusive manner, where $\alpha = 0.5$ or less. The mean α values of the MSD curves from Figure 2 were 0.2, 0.13, and 0.1 for the high, intermediate, and low swelling gels, respectively. These low α values are due to the NPs moving within a confined region. Although the calculated meshes of these gels in the fully swollen state at 22 °C were larger than the NP diameter, NPs were unable to diffuse freely, i.e., Brownian diffusion.

To quantify the localization regions which confined the NPs, van Hove displacement distributions were determined (Figure 4).[33−36] The displacement distributions describe the probability of a particle moving a distance, x, along a single axis within a specific time interval, τ. The distributions were determined using[33]

$$\Delta = x(t + \tau) - x(t) \tag{6}$$

Times of 0.08 (blue) and 1 s (red) were selected to cover the time range shown for the MSD curves in Figure 3. The displacement distributions at an intermediate time, 0.4 s, were also determined but were omitted for clarity. Figure 4a shows that small displacements occur with a higher probability than large displacements. The displacements of NPs within the low swelling gel are time-independent, as noted by the overlap of the 0.08 and 1 s displacement distributions. As polymer content decreased (intermediate swelling gel), NP displacements began to show time-dependent behavior; the spread of the displacement distributions slightly increased from 0.08 to 1 s. Upon further decreasing cross-linker content (high swelling gel), larger displacements were observed, as noted by the broader distribution and displacements greater than 200 nm at 1 s.

Displacement distributions were fit with Gaussian distributions to extract the full width at half-maximum (FWHM), which represents the localization regions. The confined motion of the NPs in NIPAAM allowed the displacement distributions to be well fit by Gaussian functions. Single and double Gaussian fits were compared with the experimental data to determine which was appropriate using r^2 and the position of the center of the peak as criteria for best fit (Table 2). The FWHM values are displayed as a histogram in Figure 5, where the FWHM's at 0.08 and 1 s are shown as blue and red bars, respectively, and the primary and secondary localization regions are shown as solid and crosshatched bars, respectively. NP displacements within the low swelling gel were well fit by a single Gaussian, while the displacements within the intermediate and high swelling gels were best fit with double Gaussians. Italic values in Table 2 denote better quality fits as determined by r^2 and position of the center of the Gaussian. This analysis suggests that NP "probes" are confined by two barriers, resulting in a narrow primary localization region and a broader secondary region. Within the low swelling gel, the primary localization region did not change with time, consistent with the time-independent behavior of the displacements. In the intermediate swelling gel, the primary localization region increased by less than 20 nm from 0.08 to 1 s, whereas the secondary localization region increased by almost 50 nm over the same time. In the high swelling gel, the primary localization region increased by 10 nm from 0.08 to 1 s, while the secondary localization region increased by over 50 nm over the same time. As polymer and cross-linker contents were reduced, the primary localization region increased only slightly, by 20 nm or less. The secondary localization region, however, increased by over 40 nm at 1 s from NPs within the intermediate and high swelling gels.

DOI: 10.1021/acs.macromol.8b00335
Macromolecules 2018, 51, 3597−3607

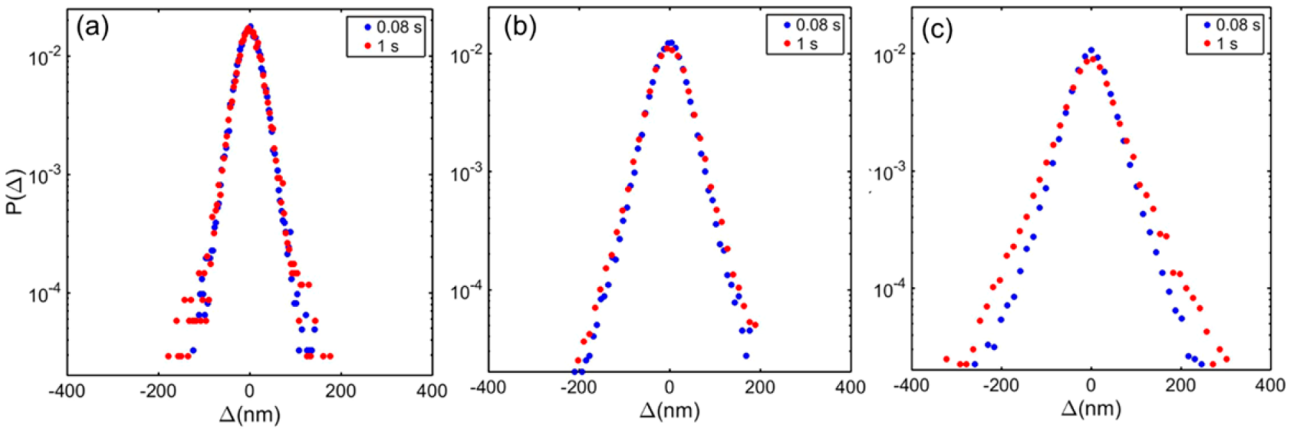

Figure 4. Van Hove displacement distributions of NPs in (a) low, (b) intermediate, and (c) high swelling gels at 0.08 (blue) and 1 (red) s at 22 °C. Distributions were fit with single/double Gaussians to determine the size of the primary and secondary localization regions, which are plotted in Figure 5.

Table 2. FWHM and Goodness of Fit for Single and Double Gaussian Fitting to the Van Hove Distributions for Each Gel Type and Temperature[a]

			single Gaussian		double Gaussian		
sample	time (s)	temp (°C)	FWHM (nm)	r^2	FWHM (nm)	FWHM (nm)	r^2
low	0.08	22	*78*	*0.996*	77	42	0.9966
	1		*79*	*0.9942*	77	54	0.9953
intermediate	0.08	22	106	0.9959	*81*	*152*	*0.9996*
	1		116	0.9967	*99*	*200*	*0.9997*
	0.08	25	104	0.9921	*79*	*176*	*0.9995*
	1		114	0.9929	*91*	*215*	*0.9996*
	0.08	30	116	0.9884	*84*	*205*	*0.9995*
	1		133	0.9838	*100*	*293*	*0.9994*
	0.08	37	*88*	*0.9969*	86	59	0.998
	1		*94*	*0.9956*	92	63	0.997
high	0.08	22	124	0.9935	*89*	*187*	*0.9996*
	0.4		139	0.9907	*103*	*239*	*0.9995*
	1		144	0.9879	*100*	*242*	*0.9996*

[a]FWHM values in the sixth and seventh columns represent the primary and secondary localization.

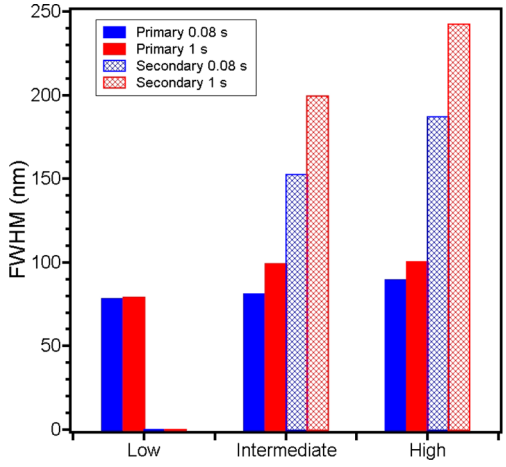

Figure 5. FWHM primary (solid) and secondary (crosshatch) localization regions determined from Gaussian fitting of displacement distributions of the low, intermediate, and high swelling gels at 22 °C for times of 0.08 s (blue) and 1 s (red). Single Gaussians best fit the low swelling gel, and therefore no secondary value is given.

As demonstrated by the tracks in Figure 2, several NPs were able to explore a larger area than that defined by the secondary localization region. The number of NPs that explore the gel at length scales larger than the secondary localization region can be determined by calculating the number of particles in 0.04 s (i.e., the frame rate) that take "steps" larger than the FWHM of the secondary localization region at 0.08 s. Thus, if a NP moved further in one frame than the localization region expected for a two frame interval, that NP was classified as escaping the localization region. Only 10% of NPs within both the intermediate and high swelling gels escaped the secondary localization region. As seen in recent studies,[35,36] large NP displacements that occur less frequently than smaller displacements are better described by exponential functions than Gaussians. Because of the low population of NPs that escaped the secondary localization region, characteristic lengths of the exponential tails of the displacement distributions were not determined.

NPs within the NIPAAM gels were primarily localized into two regions, in contrast to the diffusive motion of NPs observed in polyacrylamide gels (PAGs) with similar mesh sizes. In both a study by the authors using PEG functionalized NPs[36] and a study by Hayward and co-workers[37] using carboxylated NPs, NPs displayed intermittently diffusive or fully diffusive motion in PAGs. The difference in NP mobility, despite mesh sizes being similar, is likely due to factors other

DOI: 10.1021/acs.macromol.8b00335
Macromolecules 2018, 51, 3597−3607

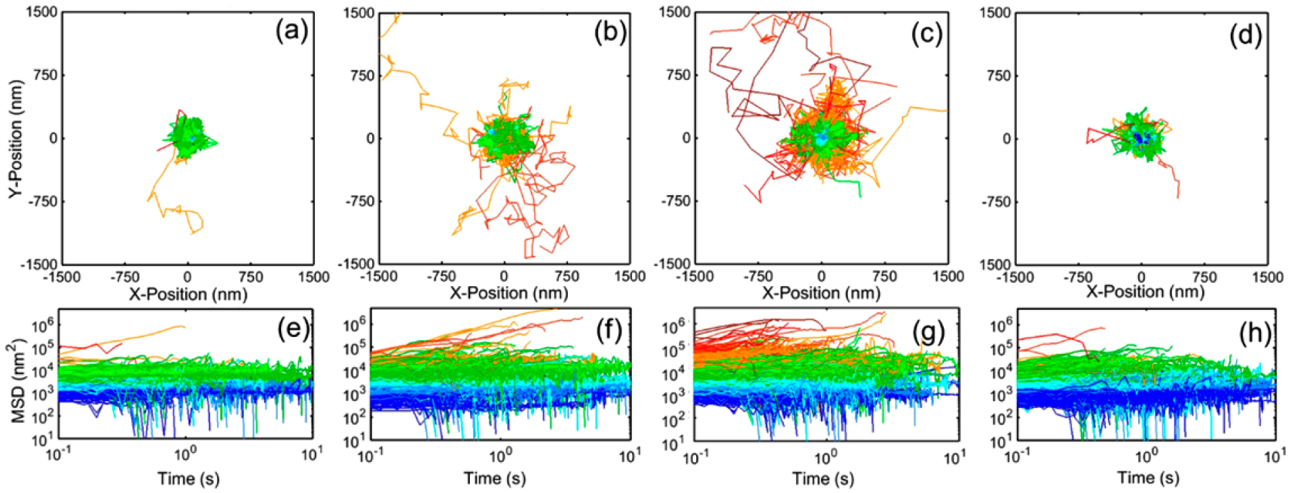

Figure 6. Trajectories of NPs in the intermediate swelling gel at (a) 22, (b) 25, (c) 30, and (d) 37 °C which have their initial location centered at (0, 0). MSDs for individual tracks as a function of time in intermediate swelling gel at (e) 22, (f) 25, (g) 30, and (h) 37 °C. Line colors vary from blue to red with increasing initial MSD (showing $N \approx 1000$).

than confinement. Additionally, charged gold NPs up to 50 nm in diameter have been shown to be mobile, at 10% of their electrophoretic mobility in water, in NIPAAM networks with similar polymer and cross-linker concentrations to the gels used in this study. The mesh sizes were determined to be in the range 6−10 nm, which is smaller than those calculated in the present study.[6] Thus, NPs less than 50 nm in size that do not interact with the chains should be mobile within the NIPAAM networks in the present study if confinement due to the mesh alone controlled mobility. The localized motion of the NPs is likely due to attractive interactions between the PEG brush on the NPs and the NIPAAM gel. A study on the swelling behavior of NIPAAM in PEG and water solutions found that NIPAAM gels deswelled and then reswelled with increasing PEG concentration, while PAGs did not reswell with increasing PEG concentration. The reswelling phenomenon was attributed to a decrease in the chi parameter between PEG and NIPAAM, from 0.4 to nearly 0 for volume fractions of PEG from 0 to 0.6. Thus, PEG acted as a good solvent due to attractive interactions between PEG and isopropyl groups of NIPAAM, which are not present on PAGs.[38]

In our study, we find that the NPs were primarily localized to a region on the order of 100 nm. We attribute this to the NPs having attractive interactions with the polymer chains, which causes them to attach and move with and along the polymer chain. This primary localization region is thus the result of both the movement of the flexible polymer chain and the movement of the NP along the chain. NPs that detach from the polymer chains remain localized by the mesh network, which results in probing a larger secondary localization region. A small number of NPs, 10% in the intermediate and high swelling gels, escape the secondary cage and move through the network until becoming localized again. This image of an interaction barrier and a network confinement barrier to NP mobility is consistent with a primary localization region that changes only slightly, but a secondary localization region that grows with decreasing polymer or cross-linker content, as seen in Figure 5.

Effect of Temperature on NP Mobility in Intermediately Swollen Gels. The intermediately swollen gel was selected for temperature dependence studies of NP mobility. Figure 6a−d displays the spatial coverage of the NP trajectories within the gel as a function of temperature. Below the VPTT, increasing temperature increased the spatial coverage of the NPs; however, above the VPTT, the spatial coverage of the NPs decreased. Lines are color coded from blue to red with increasing initial value of MSD (0.04 s). The green and blue centers of Figure 6a−d show the generally localized behavior of the NPs, with red and yellow curves, predominantly located in Figure 6b,c, depicting the trajectories of further moving NPs. The majority of NPs in the intermediate swelling gel at 22 °C were localized within a 200 nm radius. As temperature increased, the majority of NPs were localized within a radius of 260 and 350 nm at 25 and 30 °C, respectively, with a few trajectories moving distances further than 1500 nm. At 37 °C, near the VPTT, the majority of NPs trajectories were again confined to a radius of 200 nm. Overall, NPs could move greater distances with increasing temperature until above the VPTT. Quantitatively, the effect of temperature can be determined by the NP MSD curves (Figure 6e−h). As temperature was increased, a greater number of faster and further moving NPs were identified, indicated by the greater number of yellow and red MSD curves. The average MSD value at 0.4 s was $10^{3.4}$ (50^2), $10^{3.5}$ (56^2), $10^{3.7}$ (71^2), and $10^{3.3}$ (45^2) nm^2 at 22, 25, 30, and 37 °C, respectively. While swelling decreased monotonically as temperature increased, the mobility of the NPs increased as temperature approached the VPTT and decreased at temperatures above the VPTT.

The increase in ensemble NP mobility with increasing temperature prior to the VPTT can also be seen in the average MSD curves of Figure 7. The single curve at each temperature is the average of the many MSD curves shown in Figure 6e−h. The ensemble MSD at 0.4 s was 3860 (62^2) nm^2 at 22 °C. As temperature increased, the MSD value increased to 6695 (82^2) and 11445 (107^2) nm^2 at 25 and 30 °C, respectively. Above the VPTT, the ensemble MSD was reduced to below that of the NPs in the room temperature (22 °C) gel; at 37 °C, the MSD value decreased to 2835 (53^2) nm^2. Also, as temperature approached the VPTT, the ensemble MSD curves became less subdiffusive, as indicated by the slope, α. The α value changing from 0.13 at 22 °C to 0.35 at 25 and 30 °C. At 37 °C, the α value decreased to 0.12. NPs within NIPAAM gels at temperatures higher than the VPTT showed slower and more localized motion, despite the substantial increase in temperature, which would increase the mobility of NPs moving by

DOI: 10.1021/acs.macromol.8b00335
Macromolecules 2018, 51, 3597−3607

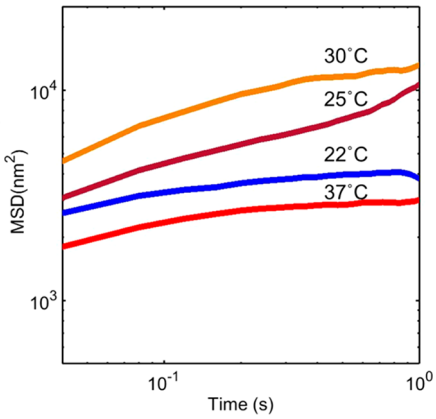

Figure 7. Ensemble NP MSD for intermediate swelling gels at 22 °C (blue), 25 °C (purple), 30 °C (orange), and 37 °C (red). Increasing temperature increased the ensemble MSD prior to the VPTT.

Stokes−Einstein diffusion. Studies on NIPAAM microgels have found that despite a monotonic change in microgel swelling with temperature through the VPTT, the modulus of the gels change nonmonotonically with temperature.[39,40] Researchers observed an increase in modulus after full collapse of the NIPAAM gels; however, through the VPTT, the microgels softened compared to the fully swollen state. Here we also observe a monotonic decrease in gel size (Figure 1) accompanied by nonmonotonic behavior in NP mobility. Through the VPTT, where other researchers observed a decrease in modulus,[39,40] we observed an increase in NP mobility.

For NPs within the intermediate swelling gel, the van Hove displacement distributions as a function of temperature are shown in Figure 8. For each temperature, the displacement distributions at 0.08 and 1 s are shown in blue and red, respectively. Figure 8a shows that the majority of the displacements are small, indicated by the high probability of

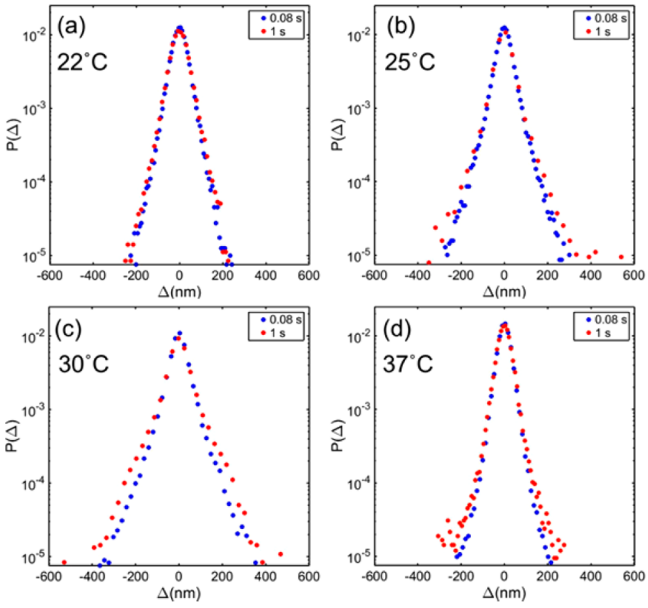

Figure 8. Van Hove distributions of NPs in the intermediate swelling gel at (a) 22, (b) 25, (c) 30, and (d) 37 °C at 0.08 s (blue) and 1 s (red).

displacements around 0 nm, and larger displacements occur with decreasing likelihood. The increased displacements of NPs with increasing temperature from 22 to 30 °C can be seen from Figure 8a to 8c. At 22 °C, the largest displacements at 1 s are just over 200 nm, while at 30 °C the largest displacements at 1 s are greater than 400 nm. Additionally, at temperatures below the VPTT, NP displacements are time-dependent, shown by the spread of the distributions increasing from 0.08 s (blue) to 1 s (red). At intermediate times, the distributions followed the same trend but were removed from the graphs for clarity. Above the VPTT, however, the displacement distribution shows negligible time dependence, seen by the overlapping blue and red data, and smaller displacements. The largest displacements at 1 s again reached just over distances of 200 nm. Interestingly, despite the 15 °C increase in temperature, the 10 nm NPs were confined similarly at 22 and 37 °C. As a reference, if the NPs were moving by Stokes−Einstein diffusion in water, the diffusion coefficient would be 1.45 times greater at 37 °C than 22 °C.

The displacement distributions were fit with Gaussian functions to determine the localization regions from the FWHM. For temperatures below the VPTT, the distributions were best fit by double Gaussians as determined by r^2 value and position of the center peak (a comparison of fit quality is shown in Table 2). Figure 9 shows the FWHM primary (solid) and

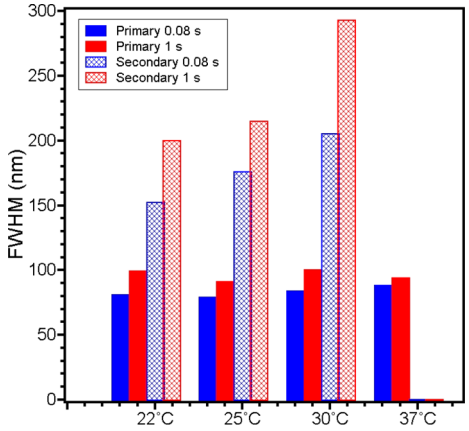

Figure 9. FWHM of the primary (solid) and secondary (crosshatch) localization regions determined from Gaussian fitting of displacement distributions of NPs in the intermediate swelling gels at 22, 25, 30, and 37 °C for times of 0.08 s (blue) and 1 s (red). At 37 °C, a single Gaussian provided a best fit consistent with a primary region only.

secondary (crosshatch) localization regions of the displacement distributions of NPs at 22, 25, 30, and 37 °C at 0.08 and 1 s. At 22 °C, the primary localization region increased from 81 to 99 nm at 0.08 and 1 s, respectively, while the secondary localization region increased from 152 to 200 nm over the same time range. As temperature was increased, the primary localization region changed very little—only 20 nm over the entire temperature range. The secondary localization region, however, increased with both temperature and time. For example, the secondary localization region at 1 s increased from 200 nm at 22 °C to 293 nm at 30 °C. Additionally, as temperature was increased, though still a minority, more NPs could escape the secondary localization region, increasing from 11% at 25 °C to 14% at 30 °C. Whereas the swelling decreased from 22 to 30 °C, the mobility of NPs increased, with secondary localization region increasing on the order of 100

DOI: 10.1021/acs.macromol.8b00335
Macromolecules 2018, 51, 3597−3607

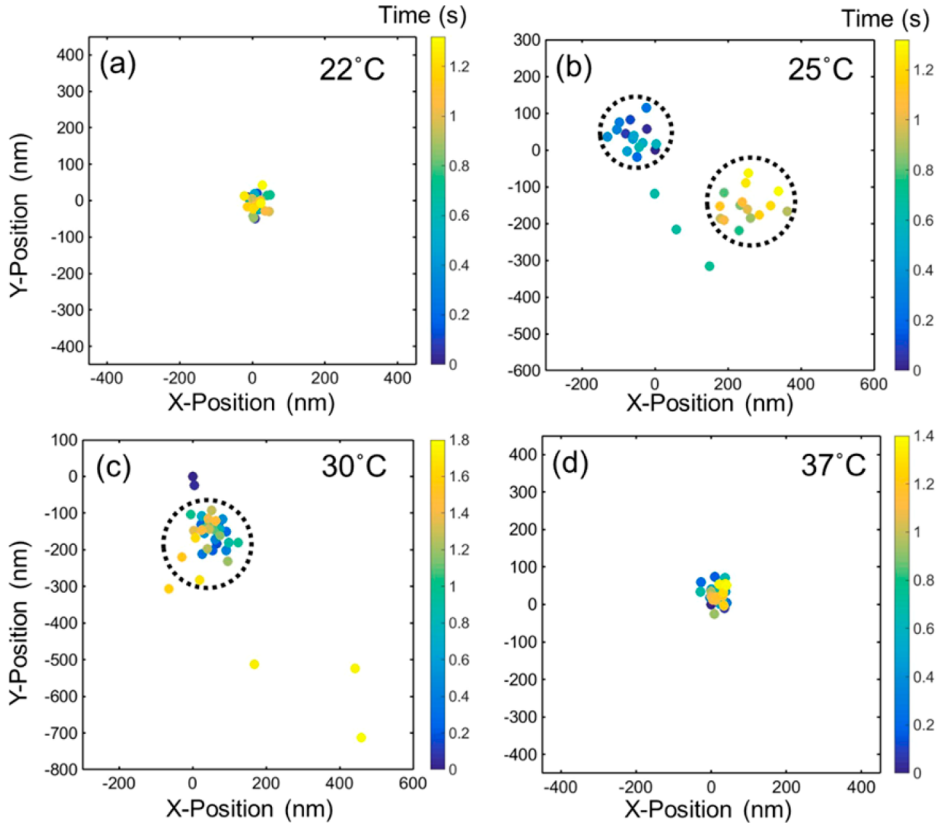

Figure 10. Example trajectories in the intermediate swelling gel at (a) 22, (b) 25, (c) 30, and (d) 37 °C. (a) and (d) display typical localized NP trajectories. (b) and (c) show trajectories of NPs that escaped the secondary localization region, which were 215 and 293 nm at 1 s, respectively. The color scale is time (s) with NP trajectories beginning in blue and ending in yellow for times of 1.2, 1.2, 1.8, and 1.4 s for (a–d), respectively. Dashed circles guide the eye toward the regions in which many small displacements were taken by the NP.

nm. Above the VPTT, however, NP mobility decreased and became independent of time. At 37 °C, the displacement distributions were well fit by a single Gaussian, which resulted in a primary localization region of approximately 90 nm at 0.08 and 1 s, because NPs were unable to escape the primary barrier to diffusion—interactions with the collapsed polymer chains.

Example trajectories of NPs in the intermediate swelling gel at 22, 25, 30, and 37 °C are shown in Figure 10. Indicated by the color changing from blue to yellow, the circles show the path of the NPs with increasing time. The areas of dense circles in the example trajectories corroborate the size of the localization regions determined from the FWHM of the displacement distributions. Figure 10a shows a NP trajectory at 22 °C which has a spatial coverage approximately equal to the primary localization region size at 1 s of 99 nm. Figure 10b shows a NP at 25 °C that escaped both the primary and secondary localization regions of 91 and 215 nm at 1s, respectively, before becoming localized again. Figure 10c shows a NP trajectory at 30 °C which also escaped the primary and secondary localization regions; however, relocalization was not observed before the NP moved out of frame. In Figure 10d, the NP trajectory covers an area approximately equal to the primary localization region size at 37 °C of 90 nm. Again, these example trajectories show that at temperatures above the VPTT, NPs are less mobile than at temperature below the VPTT.

From SPT analysis, the differences in size between the calculated mesh sizes and the primary and secondary localization regions determined was apparent. While theory and scattering studies usually determine gel meshes to be on the order of tens of nanometers,[5,7,41] studies that use NPs probes or study their diffusion often find the meshes to be larger, on the order of the localization regions found in this study.[6,36,37] The intrinsic heterogeneity of the gel structure likely explains the apparent discrepancy. As discussed in the Introduction, spatial heterogeneity within the gel network is caused by fluctuations in polymer and cross-linker content at the time of gelation. The secondary localization regions determined here describe more open areas within the network, while NPs are likely excluded from the regions with highest polymer density.

In addition to the increase in the secondary localization size with decreasing polymer and cross-linker content, we observed that the secondary localization region increased as the VPTT was approached. As temperature increased, two competing forces impacted the localization of the NPs: macroscopic deswelling and thermal energy. Thermal energy should increase the mobility of the NPs as temperature increases, whereas the macroscopic deswelling of the gel would be expected to decrease the secondary localization region by at least 15 nm as it is related to the network mesh (Table 1). A study on the electrophoretic mobility of gold nanorods in NIPAAM found that just prior to the VPTT, nanorods moved more quickly due to spinodal decomposition of the gel into polymer-rich and solvent-rich phases.[6] Here, we find that on average NPs move more quickly as the VPTT was approached as well and postulate that a similar phenomenon is happening. We visually observed a change in the turbidity of the gels as the VPTT was

DOI: 10.1021/acs.macromol.8b00335
Macromolecules 2018, 51, 3597–3607

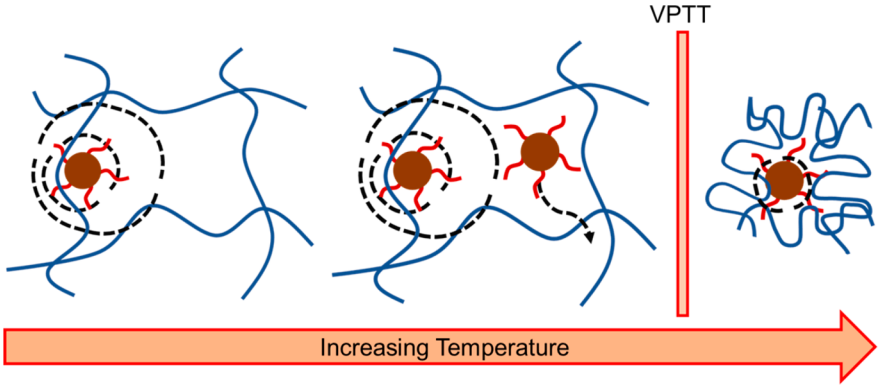

Figure 11. Schematic of the changes in mesh and NP mobility with increasing temperature. On the left, the system is at 22 °C, the gel is fully swollen, and the NPs are primarily moving in a localized manner due to interactions with the mesh, indicated by the dashed black circles. In the middle, the system is at 25−30 °C, where macroscopically the gel is contracting, while nanoscopically, the mesh is larger in polymer poor regions and smaller in polymer-rich regions. NPs are either still localized due to interactions and confinement (dashed circle) or escaping the mesh network to become localized elsewhere (dashed arrow). On the right, the system is at 37 °C, above the VPTT. The gel network has collapsed, and the NPs are localized due to attraction to the collapsed network.

approached, which is indicative of phase separation (not shown).[42] As separation of the gel into polymer- and solvent-rich domains occurs, NPs which are localized in regions with higher polymer concentration remain confined by the primary barrier to diffusion—interaction with the polymer chains. However, NPs that are localized within regions of more open network within the gel can move more due to the increased solvent in that region, driving the increase in the secondary localization region. Ultimately, however, the macroscopic deswelling and collapse of the gel dominates. Above the VPTT, at 37 °C, NPs are localized to a region smaller than at room temperature despite the increased thermal energy. The behavior of the NPs with increasing temperature is shown schematically in Figure 11. On the left, the gel, at 22 °C, is fully swollen, and the NPs are moving in a caged manner due to interactions with the polymer chains and the network confinement. The localization regions are schematically indicated by the dashed black circles. The center panel depicts the NPs behavior from 25 to 30 °C. As the gel begins to contract macroscopically, the NPs within the regions of less polymer density experience a larger secondary localization region, imposed by the mesh. Additionally, a few NPs escape the secondary localization region to eventually become localized within another mesh. On the right, the system is at 37 °C, above the VPTT, the gel network has collapsed, and the NPs are localized by the collapsed network.

CONCLUSION

The mobility of NPs functionalized with PEG brushes within NIPAAM gels that display a VPTT near body temperature was studied as a function of the swelling ratio of the gel. The swelling ratio was tuned by polymer and cross-linker content and by temperature. From our analysis, NPs were mainly localized within two barriers, resulting in a narrow primary localization region due to interaction between the PEG brush and NIPAAM chains and a broader secondary localization region due to network confinement. Our results show that increasing either polymer or cross-linker content resulted in a decreased swelling ratio, NP mobility, and secondary cage localization region. Of particular interest is how the mobility of NPs was influenced by temperature and the VPTT of these responsive gels. Increasing temperature below the VPTT resulted in increased NP mobility, secondary localization size, and percentage of NPs that could escape the secondary barrier. Above the VPTT, however, NP mobility became independent of time, indicating fully localized motion, and only a primary localization region was observed due to the collapse of the gel. Interestingly, despite the 15 °C increase in temperature, 10 nm NPs were completely localized above the VPTT. Gaining a holistic picture of gel structure and NP mobility within gels will aid in the development of materials for biomedical applications, such as injectable hydrogels where the diffusion and interaction with nanoscale drugs underpins performance.

AUTHOR INFORMATION

Corresponding Author

*E-mail composto@seas.upenn.edu (R.J.C.).

ORCID

Russell J. Composto: 0000-0002-5906-2594

Notes

The authors declare no competing financial interest.

ACKNOWLEDGMENTS

Support was provided by the NSF/CBET 1706014 (R.J.C., E.P.), NSF PIRE OISE-1545884 (R.J.C.), ACS/PRF 54028-ND7 (R.J.C., E.P.), NSF Graduate Fellowship (E.P.), and NSF/DMR 1507713 (R.J.C.). The single particle tracking experiments were performed at Scanning and Local Probe Facility at the Singh Center for Nanotechnology at the University of Pennsylvania. The authors thank Dr. Matt Brukman for instrument support, Dr. Matteo Cargnello and Dr. Christopher Murray for QD synthesis, and Benjamin Lindsay for MATLAB coding assistance.

REFERENCES

(1) Gehrke, S. H. Synthesis, Equilibrium Swelling, Kinetics, Permeability and Applications of Environmentally Responsive Gels. *Adv. Polym. Sci.* **1993**, *110*, 81−144.

(2) Kang, Y.; Joo, H.; Kim, J. S. Collapse-Swelling Transitions of a Thermoresponsive, Single Poly(*N*-isopropylacrylamide) Chain in Water. *J. Phys. Chem. B* **2016**, *120* (51), 13184−13192.

(3) Juurinen, I.; Galambosi, S.; Anghelescu-Hakala, A. G.; Koskelo, J.; Honkimäki, V.; Hämäläinen, K.; Huotari, S.; Hakala, M. Molecular-Level Changes of Aqueous Poly(*N*-isopropylacrylamide) in Phase Transition. *J. Phys. Chem. B* **2014**, *118* (20), 5518−5523.

DOI: 10.1021/acs.macromol.8b00335
Macromolecules 2018, 51, 3597−3607

(4) Kara, S.; Pekcan, Ö. Phase Transitions of *N*-isopropylacrylamide Gels Prepared with Various Crosslinker Contents. *Mater. Chem. Phys.* **2003**, *80* (2), 555−559.
(5) Crowther, H. M.; Saunders, B. R.; Mears, S. J.; Cosgrove, T.; Vincent, B.; King, S. M.; Yu, G. Poly(NIPAM) Microgel Particle Deswelling: A Light Scattering and Small Angle Neutron Scattering Study. *Colloids Surf., A* **1999**, *152* (3), 327−333.
(6) Grimm, A.; Nowak, C.; Hoffmann, J.; Schartl, W. Electrophoretic mobility of gold nanoparticles in thermoresponsive hydrogels. *Macromolecules* **2009**, *42* (16), 6231−6238.
(7) Mears, S. J.; Deng, Y.; Cosgrove, T.; Pelton, R. Structure of Sodium Dodecyl Sulfate Bound to a Poly(NIPAM) Microgel Particle. *Langmuir* **1997**, *13* (7), 1901−1906.
(8) Shibayama, M.; Tanaka, T. Small-angle Neutron Scattering study on weakly charged poly(N-isopropyl acrylamide-co-acrylic acid) copolymer solutions. *J. Chem. Phys.* **1995**, *102* (23), 9392−9400.
(9) Park, T. G.; Hoffman, A. S. Estimation of Temperature-Dependent Pore Size in Poly(*N*-isopropylacrylamide) Hydrogel Beads. *Biotechnol. Prog.* **1994**, *10* (1), 82−86.
(10) Cueille, G. Determination of "Middle Molecules" Presenting Vitamin B12 Molecular Size in Normal and Uremic Body Fluids. *J. Chromatogr., Biomed. Appl.* **1978**, *146* (1), 55−65.
(11) Chetty, A.; Kovács, J.; Sulyok, Z.; Mészáros, Á.; Fekete, J.; Domján, A.; Szilágyi, A.; Vargha, V. A Versatile Characterization of Poly(*N*-isopropylacrylamide-co-*N*,*N*′-methylene-bis-acrylamide) Hydrogels for Composition, Mechanical Strength, and Rheology. *eXPRESS Polym. Lett.* **2013**, *7* (1), 95−105.
(12) Shibayama, M.; Norisuye, T. Gel Formation Analyses by Dynamic Light Scattering. *Bull. Chem. Soc. Jpn.* **2002**, *75* (4), 641−659.
(13) Shibayama, M.; Norisuye, T.; Nomura, S. Cross-link Density Dependence of Spatial Inhomogeneities and Dynamic Fluctuations of Poly(*N*-isopropylacrylamide) Gels. *Macromolecules* **1996**, *29* (27), 8746−8750.
(14) Sayil, C.; Okay, O. Macroporous Poly(*N*-isopropyl)acrylamide Networks: Formation Conditions. *Polymer* **2001**, *42* (18), 7639−7652.
(15) Maolin, Z.; Min, Y.; Jian, S.; Jinshan, W.; Hongfei, H. Radiation Preparation and Diffusion Behavior of Thermally Reversible Hydrogels. *Radiat. Phys. Chem.* **1998**, *52* (1−6), 313−317.
(16) László, K.; Kosik, K.; Geissler, E. High-Sensitivity Isothermal and Scanning Microcalorimetry in PNIPA Hydrogels around the Volume Phase Transition. *Macromolecules* **2004**, *37* (26), 10067−10072.
(17) Constantin, M.; Cristea, M.; Ascenzi, P.; Fundueanu, G. Lower Critical Solution Temperature versus Volume Phase Transition Temperature in Thermoresponsive Drug Delivery Systems. *eXPRESS Polym. Lett.* **2011**, *5* (10), 839−848.
(18) Peppas, N. A.; Reinhart, C. T. Solute Diffusion in Swollen Membranes, Part I: A New Theory. *J. Membr. Sci.* **1983**, *15* (3), 275−287.
(19) Reinhart, C. T.; Peppas, N. A. Solute Diffusion in Swollen Membranes, Part II: Influence of Crosslinking on Diffusive Properties. *J. Membr. Sci.* **1984**, *18*, 227−239.
(20) Masaro, L.; Zhu, X. X. Physical Models of Diffusion for Polymer Solutions, Gels and Solids. *Prog. Polym. Sci.* **1999**, *24* (5), 731−775.
(21) Cukier, R. I. Diffusion of Brownian Spheres in Semidilute Polymer Solutions. *Macromolecules* **1984**, *17* (2), 252−255.
(22) Ogston, A. G. The Space in a Uniform Random Suspension of Fibers. *Trans. Faraday Soc.* **1958**, *54*, 1754−1757.
(23) Amsden, B. Solute Diffusion within Hydrogels: Mechanisms and Models. *Macromolecules* **1998**, *31* (23), 8382−8395.
(24) Cai, L. H.; Panyukov, S.; Rubinstein, M. Hopping Diffusion of Nanoparticles in Polymer Matrices. *Macromolecules* **2015**, *48* (3), 847−862.
(25) Yamamoto, U.; Schweizer, K. S. Microscopic Theory of the Long-Time Diffusivity and Intermediate-Time Anomalous Transport of a Nanoparticle in Polymer Melts. *Macromolecules* **2015**, *48* (1), 152−163.
(26) Akdemir, Z. S.; Kayaman-Apohan, N. Investigation of Swelling, Drug Release and Diffusion Behaviors of Poly(*N*-isopropylacrylamide)/Poly(*N*-vinylpyrrolidone) Full-IPN Hydrogels. *Polym. Adv. Technol.* **2007**, *18* (11), 932−939.
(27) Takeda, M.; Norisuye, T.; Shibayama, M. Critical Dynamics of Cross-linked Polymer Chains near the Gelation Threshold. *Macromolecules* **2000**, *33* (8), 2909−2915.
(28) Cargnello, M.; Diroll, B. T.; Gaulding, E. A.; Murray, C. B. Enhanced Energy Transfer in Quasi-Quaternary Nanocrystal Superlattices. *Adv. Mater.* **2014**, *26* (15), 2419−2423.
(29) Ruhnow, F.; Zwicker, D.; Diez, S. Tracking Single Particles and Elongated Filaments with Nanometer Precision. *Biophys. J.* **2011**, *100* (11), 2820−2828.
(30) Tarantino, N.; Tinevez, J.; Crowell, E. F.; Boisson, B.; Henriques, R.; Mhlanga, M.; Agou, F.; Israël, A.; Laplantine, E. TNF and IL-1 Exhibit Distinct Ubiquitin Requirements for Inducing NEMO-IKK Supramolecular Structures. *J. Cell Biol.* **2014**, *204* (2), 231−245.
(31) Fänger, C.; Wack, H.; Ulbricht, M. Macroporous Poly(*N*-isopropylacrylamide) Hydrogels with Adjustable Size "Cut-off" for the Efficient and Reversible Immobilization of Biomacromolecules. *Macromol. Biosci.* **2006**, *6* (6), 393−402.
(32) Winnik, F. M. Fluorescence Studies of Aqueous Solutions of Poly(*N*-isopropylacrylamide) Below and Above Their LCST. *Macromolecules* **1990**, *23* (1), 233−242.
(33) Aufderhorst-Roberts, A.; Frith, W. J.; Donald, A. M. Micro-scale Kinetics and Heterogeneity of a pH Triggered Hydrogel. *Soft Matter* **2012**, *8* (21), 5940−5946.
(34) Wang, B.; Anthony, S. M.; Bae, S. C.; Granick, S. Anamolous yet Brownian. *Proc. Natl. Acad. Sci. U. S. A.* **2009**, *106* (36), 15160−15164.
(35) Grady, M. E.; Parrish, E.; Caporizzo, M. A.; Seeger, S. C.; Composto, R. J.; Eckmann, D. M. Intracellular Nanoparticle Dynamics Affected by Cytoskeletal Integrity. *Soft Matter* **2017**, *13* (9), 1873−1880.
(36) Parrish, E.; Caporizzo, M. A.; Composto, R. J. Network Confinement and Heterogeneity Slows Nanoparticle Diffusion in Polymer Gels. *J. Chem. Phys.* **2017**, *146* (20), 203318.
(37) Lee, C. H.; Crosby, A. J.; Emrick, T.; Hayward, R. C. Characterization of Heterogeneous Polyacrylamide Hydrogels by Tracking of Single Quantum Dots. *Macromolecules* **2014**, *47* (2), 741−749.
(38) Melekaslan, D.; Okay, O. Reentrant Phase Transition of Strong Polyelectrolyte Poly(N-isopropylacrylamide) Gels in PEG Solutions. *Macromol. Chem. Phys.* **2001**, *202* (2), 304−312.
(39) Sierra-Martın, B.; Laporte, Y.; South, A. B.; Lyon, L. A.; Fernandez-Nieves, A. Bulk modulus of poly(N-isopropylacrylamide) microgels through the swelling transition. *Phys. Rev. E* **2011**, *84*, 011406.
(40) Hashmi, S. M.; Dufresne, E. R. Mechanical properties of individual microgel particles through the deswelling transition. *Soft Matter* **2009**, *5*, 3682−3688.
(41) Hecht, A. M.; Duplessix, R.; Geissler, E. Structural Inhomogeneities in the Range 2.5−2500 Å in Polyacrylamide Gels. *Macromolecules* **1985**, *18* (11), 2167−2173.
(42) Li, Y.; Wang, G.; Hu, Z. Turbidity Study of Spinodal Decomposition of an N-Isopropylacrylamide Gel. *Macromolecules* **1995**, *28* (12), 4194−4197.

DOI: 10.1021/acs.macromol.8b00335
Macromolecules 2018, 51, 3597−3607